Infrared Spectrum and UV-Induced Photochemistry of Matrix-Isolated 5-Hydroxyquinoline

ARTICLE *in* THE JOURNAL OF PHYSICAL CHEMISTRY A · MAY 2015

Impact Factor: 2.69 · DOI: 10.1021/acs.jpca.5b03942 · Source: PubMed

3 AUTHORS, INCLUDING:

Seda Sagdinc

Kocaeli University

28 PUBLICATIONS **312** CITATIONS

SEE PROFILE

Rui Fausto

University of Coimbra

328 PUBLICATIONS **4,465** CITATIONS

SEE PROFILE

THE JOURNAL OF PHYSICAL CHEMISTRY A

Article

pubs.acs.org/JPCA

Infrared Spectrum and UV-Induced Photochemistry of Matrix-Isolated 5-Hydroxyquinoline

Nihal Kuş,*[,†,‡] Seda Sagdinc,[†,§] and Rui Fausto[†]

[†]CQC, Department of Chemistry, University of Coimbra, 3004-535 Coimbra, Portugal

[‡]Department of Physics, Anadolu University, 26470 Eskişehir, Turkey

[§]Department of Physics, Kocaeli University, Kocaeli, Turkey

Supporting Information

ABSTRACT: The structure, infrared spectrum, and photochemistry of 5-hydroxyquinoline (5HQ) were studied by matrix isolation infrared spectroscopy, complemented by theoretical calculations performed at the DFT(B3LYP)/6-311++G(d,p) level of approximation. According to the calculations, the *trans* conformer of 5HQ (with the OH group pointing to the opposite direction of the pyridine ring of the molecule) is more stable than the *cis* form (by ∼8.8 kJ mol^{-1}). The main factors determining the relative stability of the two conformers were rationalized through natural bond orbital (NBO) and charge density analyses. The compound was trapped in solid nitrogen at 10 K, and its infrared spectra registered and interpreted, showing the sole presence in the matrix of the more stable *trans* conformer. Broadband *in situ* UV irradiations ($\lambda \geq 288$ nm and $\lambda \geq 235$ nm) allowed for the observation of different chemical transformations, which started by excitation to the S_1 state of 5HQ, followed by homolytic cleavage of the O−H bond, and subsequent reattachment of the H atom to the 5HQ radical to form quinolin-5(6*H*)-one and quinolin-5(8*H*)-one. The first of these two quinolinones was found to convert to open-ring isomeric ketenes, especially when irradiation was performed at higher energy, whereas the second is rather stable under the used experimental conditions. As a whole, the observed photochemistry of matrix-isolated 5HQ closely matches those previously reported for phenol and thiophenol. A detailed mechanistic interpretation for the observed photochemical processes is here proposed, which received support from time-dependent DFT calculations.

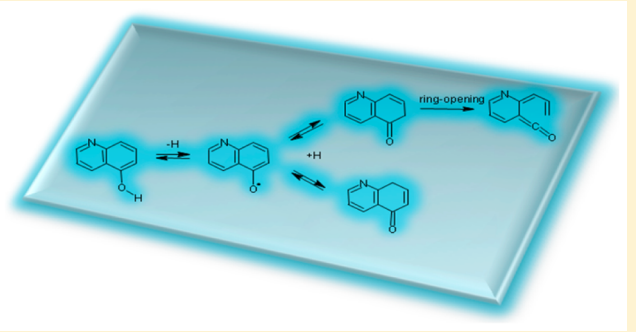

1. INTRODUCTION

Quinoline derivatives are prevalent in a variety of pharmacologically active synthetic and natural drugs.[1−6] In this field, they have been particularly successful as antimalarials, both as sole active principle and as conjugated or hybrid pharmaceuticals.[1−3] The most known quinoline derivative, quinine [or (*R*)-(6-methoxyquinolin-4-yl)((2*S*,4*S*,8*R*)-8-vinylquinuclidin-2-yl)-methanol], was widely used as first-line antimalarial in the past and is still used presently when artemisinins are not available.[7,8]

Quinolines receive also application in dyes, optics, pesticides, and fungicides industries.[9,10] In all these fields of application, the detailed knowledge of the molecular structure and spectroscopic properties of these compounds, and especially of their photochemistry, is of fundamental importance to understand their way of acting and expand their uses.

Among the quinoline derivatives, the hydroxy-substituted quinolines (HQs) have received particular attention in the last decades because they exhibit appealing chemical and physical properties: they are excellent chelating agents,[11,12] catalysts for polymerization,[13] fungicides (or direct precursors to fungicides),[14] and promising materials for photoluminescent-based optical devices.[15−17]

Because the hydroxyquinolines have both an acidic phenolic OH group and a basic nitrogen atom on the quinoline ring, these compounds are in general prone to keto−enol tautomerism, including photoinduced excited-state tautomerism.[18] Very interestingly, the relative stability of the keto and enol forms has been found to depend on the position of the OH substituent: in 2HQ and 4HQ (in which the OH group is bonded to the *ortho*- and *para*-positions of the pyridine ring, respectively) the keto form is more stable than the enol form; on the contrary, the enol is the most stable tautomer in the case of all HQs possessing the OH group connected to the benzene ring, and also in 3HQ.[19−21]

In addition, the phenolic moiety has been shown to be easily activated for O−H bond homolytic cleavage upon UV excitation under matrix isolation conditions.[22−24] For example, the parent phenol (C_6H_5OH) isolated in a solid argon matrix at 15 K has been shown to undergo facile transformation to 2,5-cyclohexadienone upon *in situ* UV irradiation ($\lambda = 275$ nm), the phenoxyl radical acting as intermediate in this reaction.[22]

Received: April 24, 2015
Revised: May 25, 2015

DOI: 10.1021/acs.jpca.5b03942
J. Phys. Chem. A XXXX, XXX, XXX−XXX

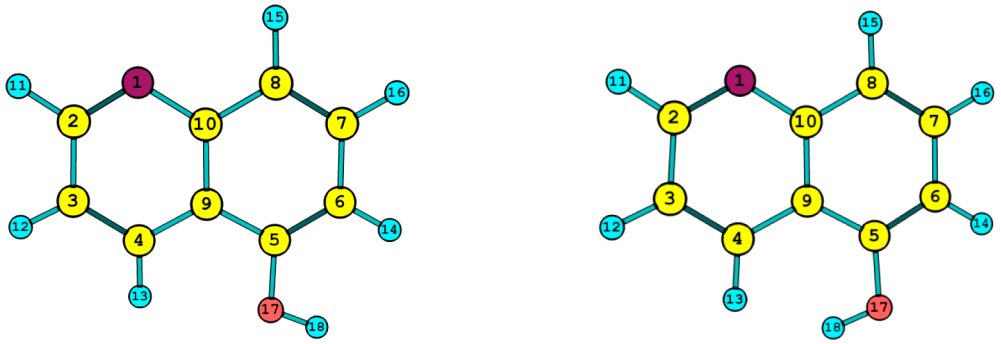

Figure 1. Conformers of 5-hydroxyquinoline (enol form) with adopted atom numbering. Conformer *cis* corresponds to the higher energy form (ΔE = 8.81 kJ mol^{-1}; $\Delta E(0)$ = 8.34 kJ mol^{-1}; $\Delta G°$ = 7.78 kJ mol^{-1}, as calculated at the B3LYP/6-311++G(d,p) level of approximation; ΔE, $\Delta E(0)$, and $\Delta G°$ are the relative electronic energy, zero-point-corrected electronic energy, and Gibbs energy, respectively).

Similar photoinduced processes, involving H atom detachment and recombination with the phenoxyl radical initially formed to yield products other than the initial reactant, have also been observed for other phenol-type compounds, like triclosan [5-chloro-2-(2,4-dichlorophenoxy)phenol][23] and 2-naphthol,[24] for example.

In the present study, we focused our attention on 5-hydroxyquinoline (5HQ; Figure 1). In this molecule, the OH substituent is located far from the ring-nitrogen atom, so that intramolecular keto−enol tautomerization involving the ring nitrogen atom as H atom acceptor cannot take place. At matrix isolation conditions, intermolecular tautomerization is also precluded. Hence, the target species corresponds to the enol tautomer of the compound. Besides the detailed study of the structure, conformational preferences and vibrational spectrum of 5HQ, in this study the photochemistry of the compound was investigated comprehensively.

The chosen experimental approach combines the matrix isolation technique[25,26] with infrared spectroscopy, supplemented by quantum chemistry calculations undertaken at a convenient level of theory [DFT(B3LYP), with the 6-311++G(d,p) basis set]. This approach has been shown[26,27] to be a very powerful strategy to elucidate structural and conformational details of isolated molecules, and also to establish mechanistic insights on their unimolecular photochemistry. First, increased resolution of the infrared spectra of matrix-isolated species is relevant when one needs to discriminate between different conformers of the same molecule, which can be expected to have rather similar spectra. This increased spectral resolution results from the quenching of the rotational transitions, hot vibrations and subtractive combination tones, and reduced inhomogeneous broadening, as well as from the virtual absence of intermolecular interactions between the matrix-isolated molecules under these experimental conditions. Second, matrix isolation stabilizes otherwise short-living reaction intermediates, opening the possibility of their study at a laboratory time scale. Third, the inherently greater simplicity of the photochemistry of a matrix-isolated molecule compared with those in gas phase or in solution results from the fact that secondary processes involving photoproduced fragments originally belonging to different molecules do not occur for the cage-confined matrix-isolated molecules. Finally, the vibrational spectrum of a molecule isolated in a cryogenic inert matrix is, most of times, practically identical to the pure vibrational spectrum of the molecule *in vacuo*, thus allowing for an easy and direct comparison of the experimental results with those obtained using state-of-the-art theoretical methods.

As will be shown in this article, isolation of 5HQ in an N_2 matrix (at 10 K) allowed us to interpret in detail its infrared spectrum, revealing the presence of a single conformer of the compound in the matrix, where the phenolic OH bond points toward the direction opposed to the pyridine ring (conformer *trans* in Figure 1). Upon consecutive broadband *in situ* UV irradiations at $\lambda \geq 288$ nm and $\lambda \geq 235$ nm, 5HQ was found to isomerize to its keto-forms, quinolin-5(6*H*)-one and quinolin-5(8*H*)-one, the first undergoing subsequent conversion to isomeric open-ring ketene species, and the second being photostable under the used experimental conditions. Mechanistic insights on the observed photochemical processes will be provided.

2. EXPERIMENTAL AND COMPUTATIONAL METHODS

5-Hydroxyquinoline (97%) was purchased from Sigma-Aldrich. Before the cryostat was cooled, the vapors over the compound in a Knudsen cell were pumped out several times, to remove possible traces of volatile impurities from the sample.

The matrixes were prepared by codeposition of 5HQ vapors with a large excess of nitrogen (N50, supplied by Air Liquide) onto the cold (10 K) CsI substrate of the cryostat (APD Cryogenics closed-cycle helium refrigeration system, with a DE-202A expander). The temperature was measured directly at the sample holder, using a silicon diode sensor connected to a digital temperature controller (Scientific Instruments, Model 9650-1), which provides accuracy of 0.1 K.

The IR spectra were recorded in the 4000−450 cm^{-1} range with 0.5 cm^{-1} resolution, on a Thermo Nicolet 6700 FTIR spectrometer, equipped with a deuterated triglycine sulfate (DTGS) detector and a KBr beamsplitter.

The matrixes were irradiated with light provided by a 500 W Hg(Xe) arc lamp (Oriel, Newport) set up to provide an output power of 300 W. Irradiations were performed either with a cutoff filter transmitting light with $\lambda \geq 288$ nm or directly through the outer quartz window of the cryostat ($\lambda \geq 235$ nm). In all irradiation experiments, an 8 cm water filter was used to prevent heating of the matrix.

The quantum chemical calculations were performed using Gaussian 09.[28] Ground-state equilibrium geometries were fully optimized at the DFT level of approximation, using the 6-311++G(d,p) basis set[29] and the B3LYP functional.[30−32] The calculated harmonic vibrational wavenumbers were uniformly

DOI: 10.1021/acs.jpca.5b03942
J. Phys. Chem. A XXXX, XXX, XXX−XXX

scaled by 0.978, to correct them for the systematic shortcomings of the applied methodology (mainly for anharmonicity). Natural bond orbital (NBO) analysis was performed accordingly to Weinhold and co-workers,[33,34] using NBO 3.1, as implemented in Gaussian 09. Energies of the low-energy excited states were calculated using the time-dependent density functional theory (TD-DFT)[35,36] at the B3LYP/6-311++G(d,p) level of approximation.

3. RESULTS AND DISCUSSION

3.1. Geometries and Relative Stability of the 5HQ Conformers. Figure 1 shows the B3LYP/6-311++G(d,p) calculated optimized geometries of the two conformers (*trans* and *cis*) of 5HQ, together with the adopted atom numbering and their relative electronic (ΔE), zero-point corrected [$\Delta E(0)$], and Gibbs ($\Delta G°$) energies. Both conformers belong to the C_s symmetry point group, bearing a planar geometry. According to the calculations, the *trans* conformer is more stable than the *cis* form by 8.81 kJ mol^{-1} (ΔE), with $\Delta E(0)$ = 8.34 kJ mol^{-1} and $\Delta G°$ = 7.78 kJ mol^{-1}. Assuming the Boltzmann distribution, the *trans* conformer shall constitute ~98% of the total conformational population in the gas phase equilibrium at room temperature. Interestingly, the *trans* conformer was also found to be the selected conformer in the neat crystalline phase of the compound, as determined by X-ray diffraction.[37]

The potential energy profile for internal rotation around the C−O bond, showing the pathway for interconversion between the two conformers of 5HQ, is presented in Figure 2. The

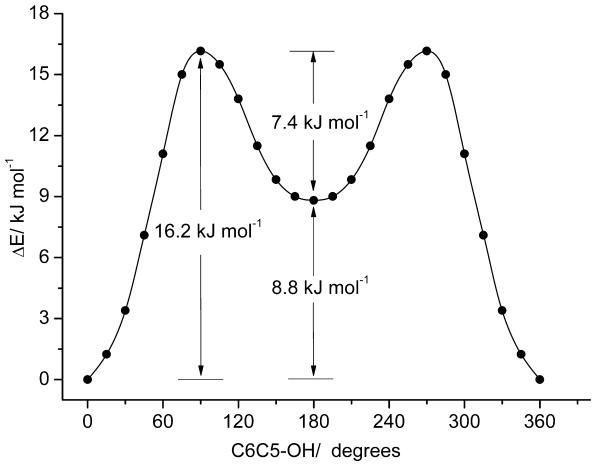

Figure 2. B3LYP/6-311++G(d,p) calculated relaxed potential energy profile for *trans*−*cis* interconversion in 5HQ (see Figure 1 for atom numbering).

predicted energy barrier for *trans* → *cis* isomerization, taken from the bottom of the potential well, is 16.2 kJ mol^{-1} (7.4 kJ mol^{-1} in the reverse direction). When the zero-point vibrational level corresponding to the isomerization coordinate (τOH) is taken into account, the *trans* → *cis* isomerization barrier is reduced to 14.5 kJ mol^{-1}, and that of the reverse process to only 6.1 kJ mol^{-1} (scaled τOH frequencies for *trans* and *cis* conformers were calculated as 288.0 and 221.7 cm^{-1}, respectively; *i.e.*, the related zero-point vibrational levels stay 1.7 and 1.3 kJ mol^{-1} above the bottom of the corresponding potential wells). The latter value is small enough to allow us to anticipate that only the more stable *trans* conformer of 5HQ shall be present in the studied cryomatrixes, the higher energy *cis* conformer being converted into the *trans* form during matrix deposition.[38]

To shed light on the main factors determining the greater stability of the *trans* conformer, compared to the *cis* form, natural bond orbital (NBO) and charge density analyses were performed. Table 1 shows the calculated natural charges on selected atoms (calculated charges for all atoms are provided in the Supporting Information, Table S1) and the main orbital interactions resulting from the second-order perturbation theory analysis of the Fock matrix, according to the NBO theory.[33,34] Additional data resulting from the performed NBO analysis are given in Tables S2 and S3 (Supporting Information).

The characteristic structural difference between the two conformers of 5HQ is the orientation of the OH group. In the more stable *trans* form, the hydroxyl H atom is directed toward H14 (Figure 1), establishing a 1−5 repulsive interaction, whereas the σ-system lone electron pair of the oxygen atom points to H13, forming a pseudo-five-membered ring. In turn, in the *cis* conformer the hydroxyl H atom is directed to H13 (1−6 repulsive interaction) and the σ-system lone electron pair of the oxygen atom points to H14, forming a pseudo-four-membered ring. The calculated atomic charges for the atoms of the C4H13−C9−C5(OH)−C6H14 fragment in the two conformers are not very different (Table 1). However, the distances between the relevant atomic charges differ considerably. Specifically, the distances between the most relevant repulsive distinctive interaction in each conformer are 2.305 Å [d(OH···H14)] and 1.956 Å [d(OH···H13)], in the *trans* and *cis* forms, respectively, whereas those between the most relevant attractive distinctive interaction are 2.479 Å [d(O:···H13), in *trans*] and 2.542 Å [d(O:···H14), in *cis*]. Both types of interactions thus favor energetically the *trans* conformer, which shows a more relevant attractive O:···H interaction and a less important repulsive OH···H interaction. A non-negligible role in determining the relative nonbonded OH···H interaction energies shall arise also from repulsive forces related to steric hindrance. For the *cis* conformer, the hydroxyl hydrogen atom and H13 are in closer contact with respect to the sum of the van der Waals hydrogen radii (~2.4 Å).

The simple qualitative analysis of the different charge interactions in the two conformers made above receives also support from the analysis of the major NBO interactions. In Table 1, NBO interactions of types A, B, and C represent interactions involving specific orbitals of the fragment that assumes a different orientation in the conformers: A-type interactions relate with the electronic charge back-donation from the σ(O−H) bonding orbital to both the σ*(C−C) antibonding orbital of the C−C bond *anti* to the O−H bond (A interaction) and the lowest energy Rydberg orbital of C5 (A′ interaction); B-type interactions are associated with the well-known[39,40] back-donation effect, through the σ-system, from the σ-type lone electron pair of the oxygen atom to the σ*(C−C) antibonding orbital of the C−C bond *anti* to the O−H bond (B interaction) and also to the lowest energy Rydberg orbital of C5 (B′ interaction); C-type interactions describe the π-delocalization between the π-type lone electron pair of the oxygen atom and the ring system. On the whole, these NBO interactions directly involving the OH fragment account for ~60% of the stabilization of the *trans* conformer in relation to the *cis* form. Interactions of type-D represent the π-delocalization within the rings, which is indirectly affected by

DOI: 10.1021/acs.jpca.5b03942
J. Phys. Chem. A XXXX, XXX, XXX−XXX

Table 1. Selected B3LYP/6-311++G(d,p) Calculated Natural Atomic Charges (e) and Main NBO Interactions ($E(2)$, kJ mol^{-1}) for *Cis* and *Trans* Conformers of 5HQ[a]

cis		*trans*	
atom	natural atomic charge	atom	natural atomic charge
C4	−0.148	C4	−0.134
C5	0.338	C5	0.368
C6	−0.254	C6	−0.300
C9	−0.141	C9	−0.146
H13	0.182	H13	0.224
H14	0.224	H14	0.201
O17	−0.685	O17	−0.678
H18	0.464	H18	0.472

	cis			*trans*		
NBO interaction	donor NBO	acceptor NBO	$-E(2)$	donor NBO	acceptor NBO	$-E(2)$
A	σ(O−H)	σ^*(C5−C6)	15.3	σ(O−H)	σ^*(C5−C9)	16.4
A′	σ(O−H)	Ry*(C5)	11.5	σ(O−H)	Ry*(C5)	9.5
B	σLp(O)	σ^*(C5−C9)	19.3	σ_{Lp}(O)	σ^*(C5−C6)	23.2
B′	$\sigma\pi_{Lp}$(O)	Ry*(C5)	10.5	σ_{Lp}(O)	Ry*(C5)	11.4
C	π_{Lp}(O)	π^*(C5−C6)	92.8	π_{Lp}(O)	π^*(C5−C6)	118.5
C′	π_{Lp}(O)	Ry*(C5)	6.6	π_{Lp}(O)	Ry*(C5)	8.7
D	π(ring)	π^*(ring)	835.4	π(ring)	π^*(ring)	857.2

[a]1e = 1.60217657 × 10^{-19} C. See Figure 1 for atom numbering and structures of the conformers. Lp, lone-electron pair; Ry*, Rydberg-type orbital. The NBO interaction designated as type D corresponds to the sum of the interactions involving ring bonding NBOs, as donors, and ring antibonding NBOs, as acceptors.

the change in the orientation of the OH group in going from one conformer to the other. They represent ∼40% of the energy stabilization of the *trans* form relatively to the *cis* conformer.

One can also divide the NBO energy stabilization of the *trans* form in terms of σ and π contributions. As shown in Table 1, the π contribution is clearly dominant, accounting for ∼93% of the energy stabilization, versus only ∼7% due to the σ NBO interactions.

The NBO polarization of the bonding orbitals associated with the O−H, C6−H14, and C4−H13 bonds (expressed in terms of percentual contribution of atomic orbitals of the atoms forming the bond to the corresponding NBO; see Tables S2 and S3, Supporting Information) provides additional evidence of distinctive electronic density distribution features in the two conformers that can be correlated with the relative charges on the hydroxyl H atom, H13 and H14 in the two forms. In one turn, the more positive charge on H14 in the *cis* conformer (0.224 *e*, vs 0.201 *e* in the *trans* form) correlates with a greater σ(C6−H14) NBO polarization toward C6 in this conformer (C6, 61.23%; H14, 38.77%) compared to the *trans* form (C6, 60.13%; H14, 39.87%), due to the presence in the *cis* conformer of the O:···H14 interaction (replaced in the *trans* form by the OH···H14 one; Figure 1). On the contrary, the more positive charge on H13 in the *trans* conformer (0.224 *e*, vs 0.182 *e* in the *cis* form) correlates with a greater σ(C4−H13) NBO polarization toward C4 in this conformer (C4, 61.29%; H13, 38.71%) compared to the *cis* form (C4, 59.21%; H13, 40.79%), due to the presence in the *trans* conformer of the O:··· H13 interaction (replaced in the *cis* form by the OH···H13 one; Figure 1). Finaly, the slightly more positive charge of the hydroxyl H atom in the *trans* conformer (0.472 *e*, vs 0.464 *e* in the *cis* form) correlates with the greater σ(O−H) NBO polarization toward the O atom in this conformer (O, 73.90%; H, 26.10%) compared to the *cis* form (O, 73.60%; H, 26.40%), due to the stronger OH···H interaction in the *cis* conformer compared to *trans* that is a consequence of the shorter OH···H distance in the former conformer (see discussion above).

3.2. Infrared Spectrum of Matrix Isolated 5HQ. In the present study, monomers of 5HQ were isolated in a low temperature (10 K) N_2 matrix as described in section 2. The obtained infrared spectrum is shown in Figure 3, where it is compared with the B3LYP/6-311++G(d,p) calculated infrared spectra of the two conformers of the compound. In consonance with the expectations (see above), the obtained data are consistent with the sole presence of the more stable *trans* conformer in the matrix, the whole experimental spectral pattern (in terms of both frequencies and relative band intensities) being better reproduced by the theoretical spectrum of this conformer. For example, the intense characteristic feature predicted for the *cis* conformer at 1172.8 cm^{-1} (δC−O−H; Table 2) does not fit with the experimental pattern.

Table 2 presents the proposed band assignments, which were based on the comparison between the experimental spectrum and that calculated for the *trans* conformer. The good agreement between the two spectra made the assignments straightforward. Here, we discuss briefly only the assignments done for the characteristic vibrations of the OH fragment: (i) The νOH stretching vibration gives rise to a band exhibiting four components at 3624.5, 3622.7, 3621.4, and 3618.5 cm^{-1}, indicating that at least four different matrix trapping sites exist. In fact, the spectrum shows extensive band splitting in several regions, which results from the existence of spectroscopically nonequivalent trapping sites. This phenomenon is particularly noticeable for intense bands, as commonly observed. In some cases (where a larger number of component bands are observed), the band splitting results also from the simultaneous occurrence of Fermi resonances. For example, the multiplet with at least eight component bands assigned to the highest-frequency ring stretching vibration, in the 1640−1615 cm^{-1} spectral range (Table 2), results from the conjugate effect of matrix-site splitting and Fermi resonance interactions with the

DOI: 10.1021/acs.jpca.5b03942
J. Phys. Chem. A XXXX, XXX, XXX−XXX

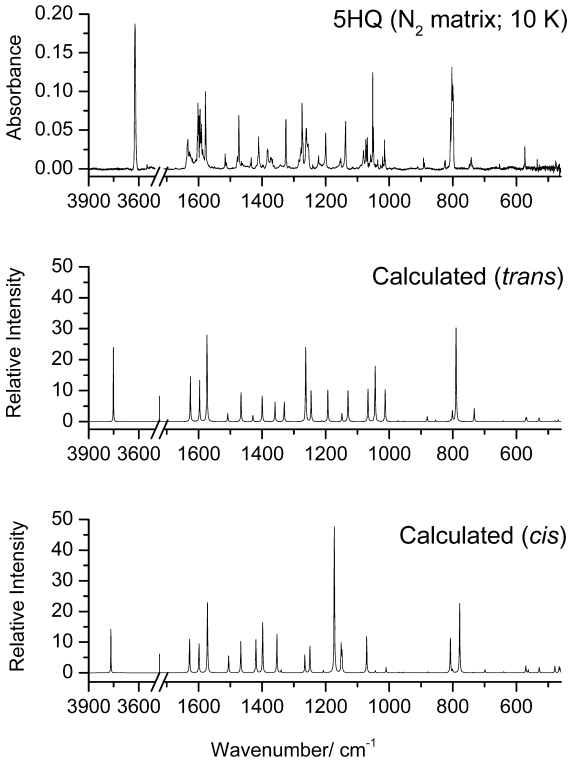

Figure 3. Infrared spectrum of 5HQ in N_2 matrix (top trace) and B3LYP/6-311++G(d,p) calculated spectra for the *trans* and *cis* conformers of the molecule (middle and bottom traces, respectively). In the calculated spectra, the wavenumbers were scaled by 0.978 and the bands were simulated by Lorentzian functions centered at the calculated frequencies and with a full-width at half-maximum (fwhm) of 2 cm^{-1}.

overtones and combination tones of appropriate symmetry (A′) of the ring torsional and deformational vibrations and γCH (all-in-phase mode) whose fundamentals are observed in the 825−798 cm^{-1} region. (ii) The νC−O stretching mode is observed as a multiplet in the 1285−1270 cm^{-1} range, with at least nine component bands and the highest maximum at 1274.4 cm^{-1} (Table 2 and Figure 3). The observed band structure results from matrix-site splitting and Fermi resonance interactions with overtones and combination tones of the modes with fundamental frequencies in the 650−550 cm^{-1} region [δ(ring) and τ(ring) modes; Table 2]. (iii) Rather interestingly, the spectroscopic feature ascribable to the δC−O−H in-plane vibration is essentially a single asymmetrical band. This indicates that the splitting due to different matrix trapping sites is, for this vibration, much smaller, resulting in nonresolved bands. (iv) The remaining vibrations of the OH fragment (τOH, δCCO and γCO) were predicted to occur, in the *trans* conformer of 5HQ, at 288.0, 282.0, and 244.9 cm^{-1}, *i.e.*, all lying well below the investigated spectral region (>450 cm^{-1}).

3.3. UV-Induced Reactions of Matrix Isolated 5HQ. The photochemistry of matrix-isolated (argon) 6- and 7-hydroxyquinolines (6HQ; 7HQ) has been investigated by Sekine et al.[20] Those authors concluded that irradiation at ∼300 nm led to production of the corresponding quinolinoxyl radicals and ketene compounds, resulting from elimination of a hydrogen atom or a hydrogen molecule, respectively.[20] In the case of 7HQ, a small amount of the keto form was also observed. For both molecules, the formation of the closed-ring ketene-6 was postulated (as a minor product), accompanied by the major production of the closed-ring ketene-5, in the case of 6HQ, or ketene-7, for 7HQ (Figure S1, Supporting Information). From these observations, the authors concluded that the initially assumed conformation of the reactants (in both cases, determined to be that where the hydroxylic hydrogen atom points to outside of the rings) plays an important role in the photoproduction of the ketenes through biradicals in a Wolff type rearrangement similar to those previously found for 2-halogenated phenols and α-diazoketo compounds.[41−45] The assumption made was that the elimination of the H_2 molecule should occur preferentially by combination of the hydroxyl hydrogen atom of the quinoline with the ring hydrogen atom located in the side toward which the hydroxyl group is oriented (Figure S1, Supporting Information). To support their conclusions, Sekine et al.[20] examined also the results of a similar UV irradiation of 5HQ, which, according to those authors, should lead to the exclusive formation of the closed-ring ketene-5 (Figure S1, Supporting Information). Very unfortunately, the assignment of the ketenes' structures was made essentially on the basis of the analysis of one spectral region (around 2240 cm^{-1}), where the very intense νC═C═O antisymmetric stretching absorbs. In addition, the possibility of formation of open-ring ketene species was not taken into account.

In relation to the putative formation of a small amount of the keto form of 7HQ, Sekine et al.[20] assumed a mechanism involving the intramolecular H atom transfer from the OH group of the quinoline to the ring N atom. The nonobservation of the keto form in the case of 6HQ was explained in terms of the longer distance the H atom would have to travel to reach the N atom for this molecule.

The recent photochemical studies on phenol,[22] the phenol derivative triclosan,[23] and thiophenol[46] opened new perspectives on the photochemistry of this type of compound when isolated in cryogenic matrixes. In these recent studies,[22,23,46] it was found that the primary event following UV absorption is H atom elimination of the OH (or SH) group, leading to the formation of the corresponding phenoxyl (or phenylthiyl) radical. This is followed by reattachment of the H atom to the ring, which may in principle occur in different positions of the ring, to form isomeric keto forms (Figure S2, Supporting Information). The keto form resulting from reattachment of the H atom to the *ortho* positions of the ring may then undergo ring-opening, leading to the production of open-ring ketene species. Such a mechanism has been solidly established on the basis of selectively induced photoisomerizations of the intervenient species by using laser irradiation at different wavelengths.[22,46]

In the present study, matrix-isolated 5HQ was subjected to broadband UV-irradiation at different cutoff transmitting conditions ($\lambda \geq 288$ nm and $\lambda \geq 235$ nm), as detailed in section 2.

Figures 4−6 show different spectral regions of the infrared difference spectra obtained by subtracting the spectrum of the initially prepared 5HQ N_2-matrix to those of the same sample after irradiation for 1 h at $\lambda \geq 288$ nm and after subsequent irradiation for 20 min at $\lambda \geq 235$ nm. The comparison of the experimental spectra of the irradiated matrix with the calculated spectra of quinolin-5(6*H*)-one and quinolin-5(8*H*)-one, which are shown in the bottom panels of these figures (see also Figure 7 for structures of the photoproducts, and Table 3 for detailed assignments), doubtlessly allowed us to conclude that these two

DOI: 10.1021/acs.jpca.5b03942
J. Phys. Chem. A XXXX, XXX, XXX−XXX

Table 2. Assignment of the Observed IR Spectrum of 5HQ (N_2 Matrix, 10 K) and B3LYP/6-311++G(d,p) Calculated Spectra for *Trans* and *Cis* Conformers[a]

Observed	Calculated[b] *trans*		*cis*		Approximate assignment[c]
ν	ν	I^{IR}	ν	I^{IR}	
3624.5/ 3622.7/ 3621.4/ 3618.5	3751.4	77.4	3767.0	45.1	νOH
3084.4	3133.3	0.4	3134.6	5.0	νCH
	3133.3	12.1	3124.9	4.7	
3077.6	3113.9	8.2	3122.3	12.7	
3072.3	3108.8	8.7	3105.0	7.7	
3043.6	3083.1	15.3	3075.0	18.3	
	3066.7	25.9	3069.6	19.1	
1637.3/ 1635.3/ 1633.5/ 1628.3/ 1625.2/ 1623.2/ 1621.6/ 1618.8	1625.8	46.0	1628.5	34.3	ν(ring)
1603.8/ 1601.6/ 1599.3/ 1597.2	1596.8	41.8	1598.8	29.9	ν(ring)
1594.7/ 1591.6/ 1590.5/ 1586.9/ 1578.0/ 1577.2	1573.5	89.2	1572.1	72.2	ν(ring)
1516.1/ 1512.3	1508.1	8.0	1505.5	17.6	ν(ring)
1479.3/ 1477.7/ 1473.3/ 1464.8/ 1461.5	1466.4	29.6	1467.2	32.3	ν(ring)
1437.0/ 1434.9/ 1434.1	1429.2	6.3	1419.4	35.1	δCH
1413.4/ 1411.1/ 1409.5/ 1407.2/ 1405.7	1399.7	26.1	1398.4	51.7	δCH
1383.8/ 1381.9/ 1378.2/ 1376.9/ 1373.8/ 1371.6/ 1370.4/ 1367.0	1359.4	20.4	1353.6	39.5	ν(ring)
1327.2/ 1325.6/ 1325.0/ 1322.4	1330.4	20.1	1340.3	2.9	ν(ring)
1284.4/ 1282.4/ 1280.2/ 1278.3/ 1277.2/ 1274.4/ 1273.9/ 1272.7/ 1271.4	1262.8	75.9	1265.6	18.4	νC–O
1261.6/ 1260.3/ 1258.3/ 1256.2/ 1255.4/ 1253.9	1245.9	32.2	1249.6	27.2	ν(ring)
1222.2	1212.8	0.9	1207.2	2.2	δCH
1200.0	1193.1	32.6	1172.8	149.7	δC–O–H
1155.2/ 1152.5	1149.0	8.3	1151.4	28.9	δCH
1139.0/ 1138.0/ 1137.2	1129.8	32.1	1148.8	20.2	δCH
1081.2/ 1073.6/ 1069.1	1067.1	33.3	1071.2	37.5	δCH
1058.4/ 1052.2/ 1049.7	1044.4	56.1	1044.0	2.1	ν(ring)
1020.7/ 1015.0/ 1012.2	1013.1	32.4	1010.1	5.7	ν(ring)
	973.5	1.0	968.2	0.6	γCH
	954.5	0.4	956.4	0.7	γCH
	948.5	0.2	925.4	0.2	γCH
892.0/ 889.4	880.8	5.2	878.1	1.0	δ(ring)
	854.5	1.5	884.6	0.1	γCH
825.8/ 824.1	807.7	1.4	808.0	35.2	τ(ring)
808.2/ 807.3	801.5	10.8	801.0	3.1	δ(ring)
803.2/ 801.8/ 799.7/ 798.9/ 798.0	789.8	98.7	778.7	71.2	γCH *(all in phase)*
748.2/ 743.4/ 742.1/ 740.2	732.6	14.0	735.6	0.5	γCH
	699.3	0.3	699.0	3.5	δ(ring)
652.9	641.3	0.8	639.9	1.2	τ(ring)
573.5	570.7	3.1	570.6	7.1	δ(ring)
	568.1	4.1	563.0	3.5	τ(ring)
534.9	529.0	4.0	528.3	5.7	δ(ring)
484.6	479.1	1.0	479.3	6.8	δ(ring)
476.5	469.1	1.8	466.0	6.0	δ(ring)
	458.4	0.4	462.8	4.5	τ(ring)
	420.9	0.8	417.3	2.7	τ(ring)
	288.0	74.4	221.7	90.9	τOH
	282.0	9.8	297.1	6.3	δCCO
	244.9	23.8	251.5	9.8	γCO
	175.0	5.9	174.6	0.1	τ(ring) *(butterfly)*
	132.5	5.7	112.5	2.0	τ(ring)

[a]Wavenumbers (ν) in cm^{-1}, IR intensities (I^{IR}) in km mol^{-1}; the spectrum was not measured below 400 cm^{-1}. [b]Calculated wavenumbers have been scaled by 0.978. [c]ν, stretching; δ, bending; γ, out-of-plane bending; τ, torsion: description of the modes is based on the major coordinate contributor; the ring stretching and CH−bending modes are extensively mixed.

molecules correspond to the two major photoproducts of 5HQ subjected to the present experimental irradiation conditions.

Quinolin-5(6*H*)-one and quinolin-5(8*H*)-one are the equivalent species of the previously observed keto forms of phenol and thiophenol,[22,46] clearly demonstrating that the UV-induced photochemistry of the matrix-isolated 5HQ follows closely that of these compounds. The whole set of photoinduced processes observed for 5HQ in the present study is shown schematically in Figure 7. As for phenol and thiophenol,[22,46] the primary phototransformation of 5HQ, after UV absorption, is the formation of the corresponding radical, by cleavage of the O−H bond, accompanied by release of an H atom. The spectroscopic identification of the 5HQ radical (quinolin-5-yloxidanyl) was complicated by the low intensity of the infrared bands of this species (with a few exceptions, predicted to be below 10 km mol^{-1}; see Figure S3, Supporting Information) and also because the concentration of the radical all along the performed irradiations was kept rather small. Nevertheless, the most

DOI: 10.1021/acs.jpca.5b03942
J. Phys. Chem. A XXXX, XXX, XXX−XXX

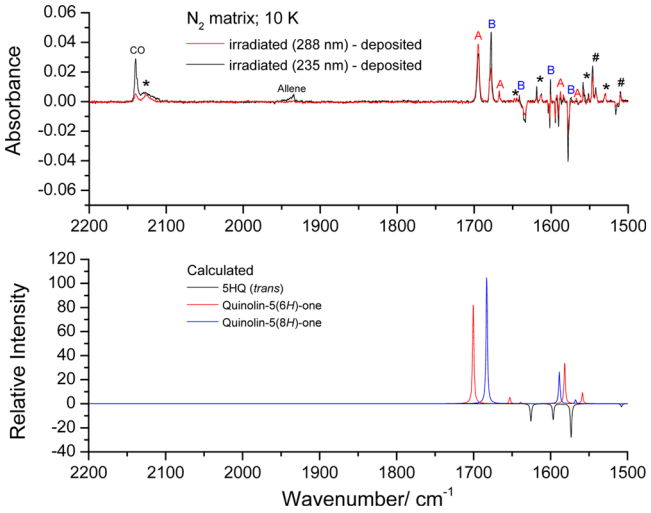

Figure 4. (Bottom) B3LYP/6-311++G)d,p) calculated infrared spectra (2200−1500 cm^{-1} region) for quinolin-5(6*H*)-one, quinolin-5(8*H*)-one, and 5HQ (*trans* form). (Top): infrared difference spectra (2200−1500 cm^{-1} region), irradiated matrix ($\lambda \geq 288$ nm; 1 h) *minus* the deposited matrix, and irradiated matrix (additional irradiation at $\lambda \geq 235$ nm by 20 min) *minus* the deposited matrix. In the experimental difference spectra, A and B designate bands of quinolin-5(6*H*)-one and quinolin-5(8*H*)-one, respectively, * indicates bands assigned to open-ring ketene isomeric species, and # identifies bands assigned to the 5HQ radical.

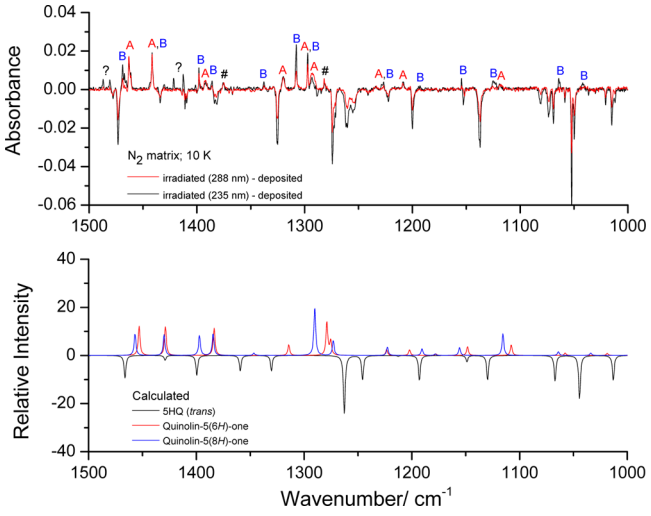

Figure 5. (Bottom) B3LYP/6-311++G)d,p) calculated infrared spectra (1500−1000 cm^{-1} region) for quinolin-5(6*H*)-one, quinolin-5(8*H*)-one, and 5HQ (*trans* form). (Top) infrared difference spectra (1500−1000 cm^{-1} region), irradiated matrix ($\lambda \geq 288$ nm; 1 h) *minus* the deposited matrix and irradiated matrix (additional irradiation at $\lambda \geq 235$ nm by 20 min) *minus* the deposited matrix. In the experimental difference spectra, A and B designate bands of quinolin-5(6*H*)-one and quinolin-5(8*H*)-one, respectively, # identifies bands assigned to the 5HQ radical, and ? refers to bands of nonidentified photofragmentation products.

intense bands of the radical, predicted at 1524, 1503, 1390, 1274, and 792 cm^{-1}, could be observed experimentally at frequencies closely located to their theoretically predicted values: 1546/1542, 1510, 1375, 1282 and in the 796−793 cm^{-1} range (Figures 4−6 and also Figure S3, Supporting Information).

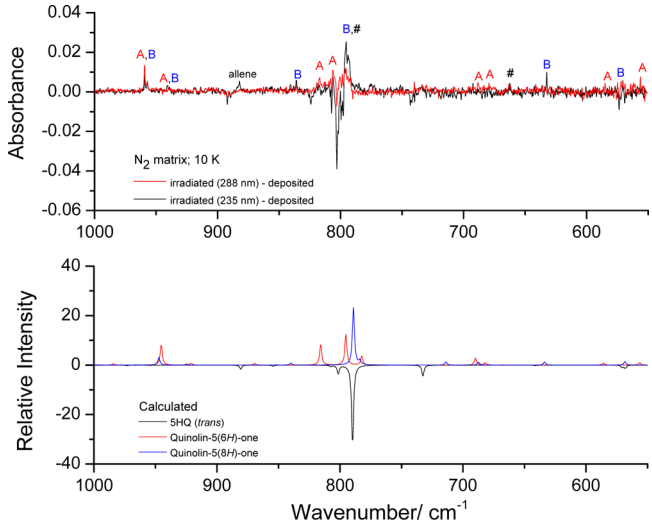

Figure 6. (Bottom) B3LYP/6-311++G)d,p) calculated infrared spectra (1000−450 cm^{-1} region) for quinolin-5(6*H*)-one, quinolin-5(8*H*)-one, and 5HQ (*trans* form). (Top) infrared difference spectra (1000−450 cm^{-1} region), irradiated matrix ($\lambda \geq 288$ nm; 1 h) *minus* the deposited matrix and irradiated matrix (additional irradiation at $\lambda \geq 235$ nm by 20 min) *minus* the deposited matrix. In the experimental difference spectra, A and B designate bands of quinolin-5(6*H*)-one and quinolin-5(8*H*)-one, respectively, and # identifies bands assigned to the 5HQ radical.

Recombination of the 5HQ radical and H atom in the original matrix cage may lead to recovering of 5HQ. The observed relatively low rate of consumption of 5HQ (1 h of irradiation at $\lambda \geq 288$ nm led to consumption of *ca.* one-half of the initially present 5HQ) indicates that the radicals recombination back-reaction is significant. On the contrary, reattachment of the H atom resulting from the initial O−H photocleavage to the *ortho* and *para* positions of the quinoline radical may also take place, leading to the observed quinolin-5(6*H*)-one and quinolin-5(8*H*)-one, respectively. These two major photoproducts were produced at different rates, with the amount of quinolin-5(6*H*)-one increasing faster than that of the quinolin-5(8*H*)-one when irradiation was performed at $\lambda \geq 288$ nm. This trend can be explained by considering a preferential attack of the H atom to the *ortho* position of the ring, which requires the H atom to travel less than when the attack occurs at the *para* position. After 1 h of irradiation at $\lambda \geq 288$ nm, the ratio of the amounts of the quinolin-5(6*H*)-one and quinolin-5(8*H*)-one photoproducts was found to be 1.2 (as estimated from the absorbances−normalized by the corresponding infrared intensities−of the bands observed at 1694.6 and 1678.2 cm^{-1}, assigned to each one of the compounds; Table 3).

When the irradiation was carried out at higher energy ($\lambda \geq 235$ nm), the amount of quinolin-5(8*H*)-one present in the sample increased relatively to that of the quinolin-5(6*H*)-one. After 20 min irradiation at $\lambda \geq 235$ nm of the sample initially irradiated at $\lambda \geq 288$ nm for 1 h, the ratio of the amounts of the quinolin-5(6*H*)-one and quinolin-5(8*H*)-one photoproducts reduces from 1.2 to 0.7 (Figures 4−6). This is essentially due to the fact that the quinolin-5(8*H*)-one demonstrated to be rather photostable under the used experimental conditions, whereas the quinolin-5(6*H*)-one is prone to undergo ring-opening to isomeric ketene forms (Figure 7), in a way similar to what was previously observed for phenol and thiophenol.[22,46]

DOI: 10.1021/acs.jpca.5b03942
J. Phys. Chem. A XXXX, XXX, XXX−XXX

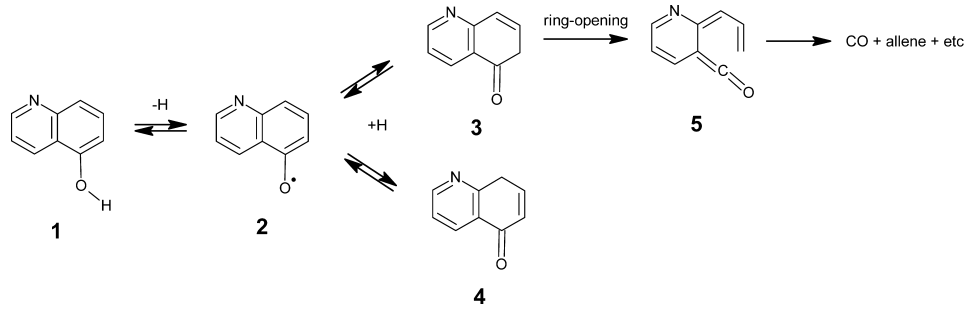

Figure 7. Observed photochemical reactions resulting from UV irradiation of 5HQ (**1**) isolated in a N_2 matrix. Initial irradiation at $\lambda \geq 288$ nm led to observation of quinolin-5(6*H*)-one (**3**, major product) and quinolin-5(8*H*)-one (**4**, minor product), via the quinolinyl radical (**2**); subsequent irradiation at $\lambda \geq 235$ nm resulted in the major production of **4**, isomeric open-ring ketene forms (**5**; for structures of the four possible isomeric forms of the ketene see Figure S4, Supporting Information), and fragmentation products (mainly CO and allene, together with other nonidentified species; see text).

In general, the spectroscopic identification of ketenes is easy because they strongly absorb in the infrared in the 2150−2100 cm^{-1} region (νC═C═O antisymmetric),[22,47,48] and such characteristic absorption is indeed observed in the spectra of the studied photolyzed 5HQ N_2-matrixes (Figure 4). However, almost all the remaining infrared bands of the ketenes that are possible to result from the photolysis of 5HQ are of low intensity (below 10 km mol^{-1}), as shown in Figure S4 (Supporting Information). Such a fact complicates the assignment of a specific structure to the ketene species formed during the discussed experiments. Besides, in general, the different possible isomeric ketene forms resulting from ring-opening reactions analogous to that taking place in the present case are formed altogether.[22,47,48] This seems also to be the current situation, considering both the considerable broadness of the observed νC═C═O antisymmetric stretching band and the multiplet structure of the other bands that were possible to assign to the ketene species (in the 1550−1500 cm^{-1} spectral region, where the next more intense bands of the ketenes are predicted to occur; see Figure S4, Supporting Information).

The amount of ketene present in the photolyzed matrix was observed to be small along all performed irradiation experiments. This can be easily rationalized: on one hand, it is produced only slowly from quinolin-5(6*H*)-one upon irradiation at $\lambda \geq 288$ nm; on the other hand, irradiation at $\lambda \geq 235$ nm not only increases the rate of the ring-opening reaction (shown by the observed consumption of quinolin-5(6*H*)-one under these irradiation conditions) but also leads to significant decomposition of the resulting ketenes, as testified by the appearance in the spectra of the $\lambda \geq 235$ nm photolyzed matrix of the characteristic bands of CO (2139 cm^{-1}),[49] allene (1938/1935 and 882 cm^{-1}),[22,50] and other nonidentified fragmentation products (*e.g.*, 1487, 1481, 1422, and 1412 cm^{-1}).

Because the photochemistry of 5HQ is rather similar to that of phenol and thiophenol,[22,46] we carefully checked the infrared spectra of the photolyzed matrix of 5HQ in search for the presence of its Dewar isomer analogous of the Dewar phenol form previously observed.[22] The Dewar 5HQ has its most intense infrared band (νC═O) predicted to occur at around 1800 cm^{-1} (Figure S5, Supporting Information), close to the observed νC═O band of the Dewar phenol isolated in an argon matrix (1789 cm^{-1}).[22] However, no band could be observed in the spectrum of the photolyzed 5HQ matrix near this spectral region, indicating that de Dewar 5HQ form was not formed in the performed experiments. Also, the species that would result from the putative reattachment of the H atom to the *meta* position the ring [quinolin-5(7*H*)-one] could be safely discarded, because no correspondence to the most intense predicted bands for this molecule (Figure S6, Supporting Information) exists in the observed spectra of the photolyzed 5HQ matrix.

The possibility of the presence, among the photoproducts of 5HQ, of the closed-ring ketene-5, previously postulated by Sekine et al.[20] as the main photoproduct of 5HQ, shall also be commented here. The calculated infrared spectrum for this ketene is shown in Figure S7 (Supporting Information), exhibiting a single intense band (predicted at 2159 cm^{-1}), with all other bands having infrared intensities below *ca.* 20 km mol^{-1} (most of them, below 10 km mol^{-1}) and, thus, being too small in intensity to allow for their experimental observation in the present experiments. Under these circumstances, it is more difficult to prove the absence of this compound among the photoproducts of 5HQ. However, there are two major pieces of information that are strong points against formation of the closed-ring ketene-5 as result of the photochemical excitation of matrix-isolated 5HQ. In the first place, the close similarity of the photochemistry of 5HQ with that of phenol and thiophenol,[22,46] as deduced by the observation of the same types of major photoproducts in all three cases, is a strong indication that the mechanism proposed by Sekine et al.[20] for the photolysis of 5HQ (describe above, and that would lead to the observation of the closed-ring ketene-5; see Figure S1, Supporting Information) is not correct. In addition, the predicted frequency for the νC═C═O antisymmetric stretching of the ketene-5 (2159 cm^{-1}) is considerably higher than those for the open-ring ketenes (between 2132 and 2125 cm^{-1}) and, contrary to these latter, expected to be higher than that of carbon monoxide (2141 cm^{-1}); as shown in Figure 4, the band of CO is in fact observed at a higher frequency than that of the broad feature due to the νC═C═O antisymmetric vibration of the ketene species produced from the photolysis of 5HQ.

In summary, all experimental and theoretical data presented and discussed above allow us to firmly conclude that the photochemistry of matrix-isolated 5HQ (summarized in Figure 7) closely follows that observed before for phenol and thiophenol,[22,46] indicating that this shall be considered a rather general photochemical behavior for matrix-isolated phenol and thiophenol derivatives.

Some additional mechanistic insights on the observed processes could also be extracted from both the analysis of the relative energies of the *a priori* possible products and time-

DOI: 10.1021/acs.jpca.5b03942
J. Phys. Chem. A XXXX, XXX, XXX−XXX

Table 3. Assignment of the Bands of Quinolin-5(6*H*)-one and Quinolin-5(8*H*)-one Observed in the Infrared Spectrum of the Photolysed 5HQ N_2 Matrix[a]

obsd[b]	calcd			
	quinolin-5(6*H*)-one		quinolin-5(8*H*)-one	
ν	ν	I^{IR}	ν	I^{IR}
2139.5 (CO)				
2129.1/2126.0/2123.9/2117.8/2112.5 (OR-K)				
1938.4/1934.9 (allene)				
1694.6	1700.7	266.9		
1678.2			1683.1	335.5
1667.3	1653.1	17.1		
1647.9/1644.6 (OR-K)				
1644.1			1639.1	3.3
1618.7/1614.0/1613.1 (OR-K)				
1600.7			1588.8	83.1
1592.4/1587.9/1583.8/1583.4	1581.9	108.8		
1574.6			1567.6	10.2
1567.4	1558.8	28.9		
1558.6/1556.6/1551.6 (OR-K)				
1546.2/1542.2 (5HQ radical)				
1529.8 (OR-K)				
1509.9 (5HQ Radical)				
1487.2/1480.7 (?)				
1468.9/1467.4/1465.8			1457.1	28.2
1463.1/1461.8	1453.3	38.3		
1441.7	1428.9	37.4	1430.1	27.2
1421.7/1412.4 (?)				
1398.3			1397.3	25.9
1391.9	1383.6	35.4		
1386.3			1384.6	28.7
1375.3 (5HQ radical)				
1337.9			1346.8	3.0
1319.8	1314.4	14.1		
1307.9			1290.2	63.0
1297.3	1279.0	43.6	1273.1	19.6
1292.8	1275.4	18.7		
1282.0 (5HQ radical)				
1233.5/1226.9	1223.5	7.8	1222.8	10.9
1208.8	1202.3	7.4		
1193.4			1190.7	8.9
1154.6			1155.8	10.5
1123.7			1115.6	28.7
1117.2	1107.8	14.1		
1063.9			1064.1	4.9
1042.0			1034.0	3.2
959.5/957.1	945.4	25.8	947.3	9.6
940.9	921.0	2.1	924.7	1.4
882.3 (allene)				
835.9			839.5	2.5
817.3	815.7	26.0		
806.2	795.3	38.8		
795.5/793.9[c]			789.1	73.3
689.1	689.9	9.0		
679.8	681.9	3.0		
663.0 (5HQ radical)				
632.5			633.7	4.1
584.9	585.8	2.7		
570.6			568.3	4.5
556.5	556.4	3.2		

[a]Frequencies (ν) in cm^{-1}. Calculated frequencies were scaled by 0.978. Calculated infrared intensities (I^{IR}) in km mol^{-1}. For full calculated infrared spectra (B3LYP/6-311++G(d,p)) of the compounds, see Table S4 in the Supporting Information. [b]Bands due to the 5HQ photolysis products in the CH stretching region have too low intensity so that they could not be assigned. [c]These bands have also a relevant contribution from the 5HQ radical.

DOI: 10.1021/acs.jpca.5b03942
J. Phys. Chem. A XXXX, XXX, XXX−XXX

Table 4. Wavelength of the Vertical Absorption (λ) and Oscillator Strength (f) Calculated Using the TD-DFT(B3LYP) Method at the Ground-State Equilibrium Geometries of 5HQ, Quinolin-5(6*H*)-one, and Quinolin-5(8*H*)-one

		5HQ			quinolin-5(6*H*)-one				quinolin-5(8*H*)-one		
state	type	λ/nm	f	state	type	λ/nm	f	state	type	λ/nm	f
S_1 (A′)	$\pi\pi$ (HOMO → LUMO)	312.3	0.050	S_1 (A″)	nπ* (HOMO → LUMO)	354.2	0.000	S_1 (A″)	nπ* (HOMO → LUMO)	358.2	0.000
S_2 (A″)	nπ*	288.1	0.002	S_2 (A′)	$\pi\pi$* (HOMO → LUMO)	315.5	0.049	S_2 (A″)	nπ*	286.8	0.000
S_3 (A′)	$\pi\pi$*	282.1	0.001	S_3 (A″)	nπ*	296.8	0.000	S_3 (A′)	$\pi\pi$* (HOMO−1 → LUMO)	269.9	0.112
S_4 (A″)	$\pi\sigma$*	255.9	0.000	S_4 (A″)	nπ*	277.4	0.002	S_4 (A″)	nπ*	261.5	0.002
S_5 (A″)	nπ*	253.0	0.000	S_5 (A′)	$\pi\pi$* (HOMO → LUMO+1)	265.8	0.131	S_5 (A′)	nπ* (HOMO−3 → LUMO)	257.3	0.085
S_6 (A″)	$\pi\sigma$*	245.3	0.000	S6 (A″)	nπ*	262.0	0.000	S_6 (A″)	nπ*	250.3	0.000
T_1 (A′)	$\pi\pi$*	456.9	0.000	T_1 (A′)	$\pi\pi$*	450.4	0.000	T_1 (A″)	nπ*	412.9	0.000
T_2 (A″)	nπ*	330.2	0.000	T_2 (A″)	nπ*	400.0	0.000	T_2 (A′)	$\pi\pi$*	374.5	0.000
T_3 (A′)	$\pi\pi$*	321.1	0.000	T_3 (A′)	$\pi\pi$*	352.4	0.000	T_3 (A′)	$\pi\pi$	342.4	0.000
T_4 (A′)	$\pi\pi$*	306.3	0.000	T_4 (A″)	nπ*	314.6	0.000	T_4 (A′)	nπ*	310.9	0.000
T_5 (A′)	$\pi\pi$*	290.9	0.000	T_5 (A′)	$\pi\pi$*	306.6	0.000	T_5 (A″)	$\pi\pi$*	297.0	0.000
T_6 (A′)	$\pi\pi$*	282.5	0.000	T_6 (A″)	nπ*	302.7	0.000	T_6 (A″)	nπ*	274.4	0.000

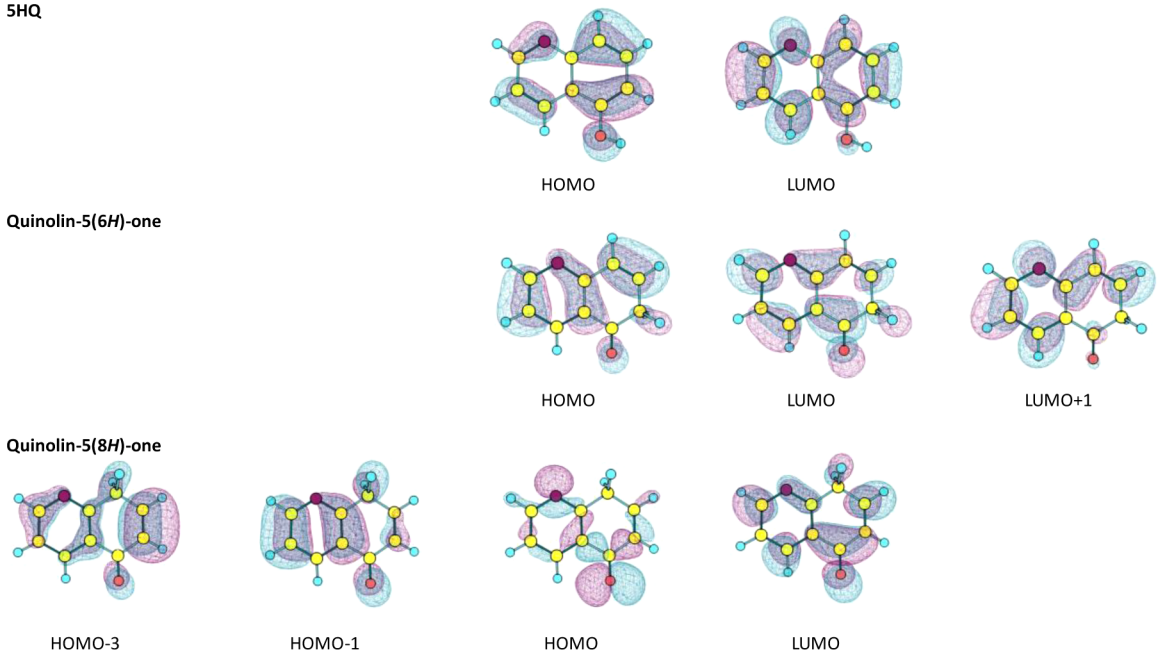

Figure 8. B3LYP/6-311++G(d,p) calculated HOMO and LUMO orbitals for 5HQ, quinolin-5(6*H*)-one, and quinolin-5(8*H*)-one, and other orbitals of these compounds participating (as acceptor or donor orbital) in the lower energy electronic transitions exhibiting a significant oscillator strength (Table 4). The depicted contour isosurfaces correspond to ±0.03 au.

dependent DFT (TD-DFT) calculations on the relevant species. These are discussed in the next section.

3.4. Mechanistic Insights on the Observed Reactions Induced by UV Irradiation of Matrix Isolated 5HQ. Table 4 presents the results of B3LYP/6-311++G(d,p) TD-DFT calculations performed on 5HQ, quinolin-5(6*H*)-one, and quinolin-5(8*H*)-one. It is clear from these results that the irradiations to which 5HQ was subjected in the present study led to excitation to the S_1 (A′) $\pi\pi$* (HOMO → LUMO) state (Figure 8 for pictures of the orbitals). The energy introduced in the molecule by this way is enough to allow for the homolytic cleavage of the O−H bond, generating the 5HQ radical plus an H atom (see also Figure 9). Indeed, such energy shall be similar to that experimentally determined for phenol, which amounts to ∼364 kJ mol^{-1}.[51−54]

The calculated relative energy for the ground state of 5HQ radical (plus H atom) is 352 kJ mol^{-1}, well above those of the two observed products resulting from reattachment of H to the *ortho* and *para* positions of the 5HQ radical, quinolin-5(6*H*)-one, and quinolin-5(8*H*)-one, respectively, which are only 36

DOI: 10.1021/acs.jpca.5b03942
J. Phys. Chem. A XXXX, XXX, XXX−XXX

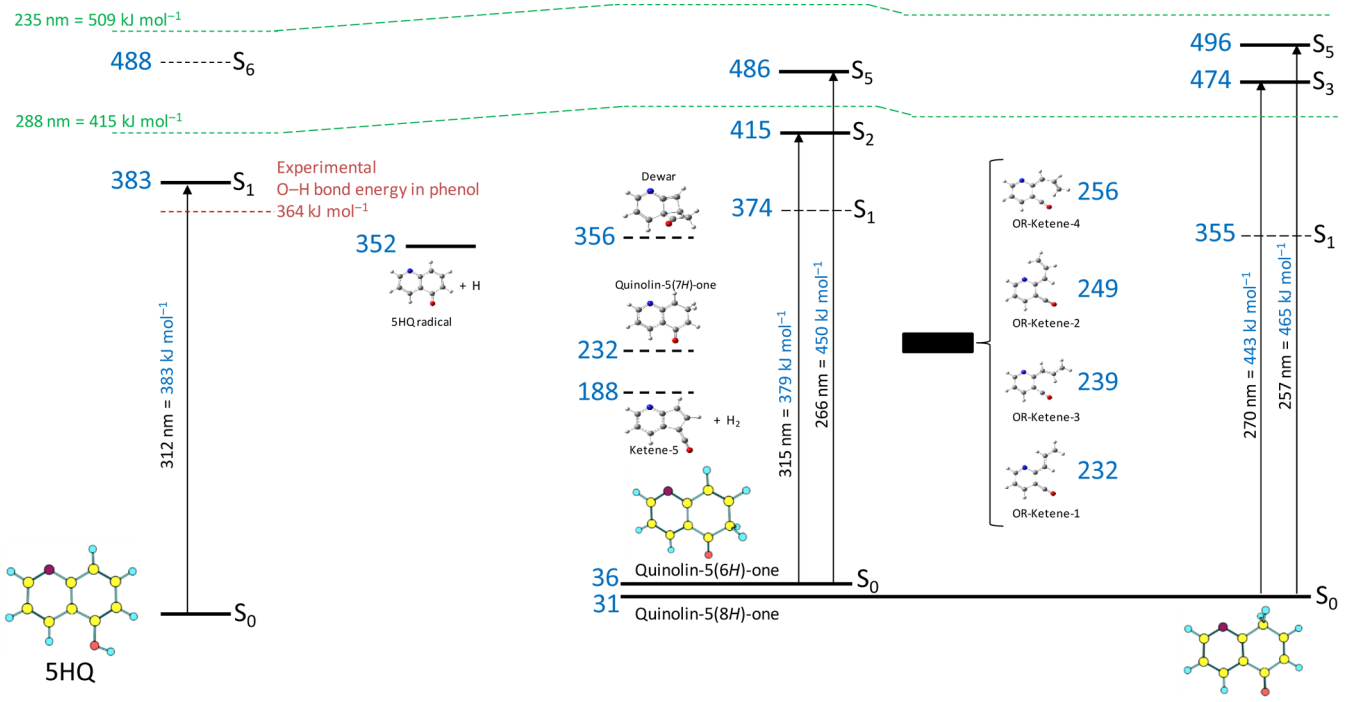

Figure 9. Summary of the B3LYP/6-311++G(d,p) energy calculations (including of excited states using the TD-DFT approach) for the species that were considered for the analysis of the UV-induced processes following excitation of matrix-isolated 5HQ. The numbers in blue are relative energies (kJ mol^{-1}) in relation to 5HQ (*trans* conformer). The green dashed lines represent the position of the cutoff wavelength in the two performed irradiation experiments in relation to the excited species: 5HQ, quinolin-5(6*H*)-one, and quinolin-5(8*H*)-one. The position of the active states of the experimentally observed compounds is represented by thick horizontal black lines, and those of other states of these compounds are represented by thin dashed horizontal lines. The position of nonobserved compounds in the energy scale is given by thick horizontal black lines. The active transitions are represented by the vertical arrows. The horizontal scale, from left to right simulates the progress of the observed reactions (note that quinolin-5(8*H*)-one is produced from reattachment of the H atom to the 5HQ radical and appeared shifted to the right in the picture to allow for representation of its excited states.) For characterization of the electronic excited states, see Table 4.

and 31 kJ mol^{-1} above that of the reactant 5HQ (Figure 9). On the contrary, the putative result of reattachment of the H atom to the *meta* position, quinolin-5(7*H*)-one, has a considerably higher energy (232 kJ mol^{-1} above 5HQ). Also, the energies of the closed-ring ketene-5 and Dewar 5HQ isomer (356 and 188 kJ mol^{-1}, respectively) are far higher than those of the observed products of recombination of the H atom with the 5HQ radical.

Once formed from 5HQ by the mechanism described above, the two quinolinones are also exposed to the effect of the ongoing irradiations. According to the TD-DFT calculations, quinolin-5(6*H*)-one has two bright states, S_2 $\pi\pi^*$ (HOMO → LUMO) and S_5 $\pi\pi^*$ (HOMO → LUMO+1), the first being accessible upon irradiation at $\lambda \geq 288$ nm and the second only upon irradiation at $\lambda \geq 235$ nm (Table 4 and Figure 9).

Both bright states of quinolin-5(6*H*)-one imply charge transfer from its HOMO to orbitals (LUMO and LUMO+1; see Figure 8 for pictures of the orbitals) where the bonding character at the C5−C6 bond π component is decreased. Such changes facilitate the occurrence of the ring-opening reaction leading to the observed open-ring ketenes. The additional excitation channel (through the S_5 state) explains the faster observed consumption of quinolin-5(6*H*)-one upon irradiation at $\lambda \geq 235$ nm. It is interesting to note that the C5−C6 bond is already intrinsically weaker than all the other C−C bonds of the molecule even in the ground electronic state, as reflected in its considerably longer length (1.524 Å) compared to those of the other C−C bonds (between 1.338 and 1.497 Å).

It can also be mentioned that the ketenes have energies well below those of the excitation energies of the quinolin-5(6*H*)-one, so that all isomeric open-ring ketene forms can be expected to be accessible as result of the photochemical reaction. This is also supported by the already mentioned broad, multicomponent appearance of the infrared features ascribable to the ketene species.

In the case of quinolin-5(8*H*)-one, according to the TD-DFT calculations two bright states [S_3 $\pi\pi^*$ (HOMO−1 → LUMO) and S_5 $\pi\pi^*$ (HOMO−3 → LUMO)] were also accessible, but only when the irradiation was performed at $\lambda \geq 235$ nm (Table 4 and Figure 9). In both cases, the acceptor orbital (LUMO) has an increased bonding character in the two C−C bonds *ortho* to the carbonyl group (Figure 8), which precludes occurrence of an efficient ring-opening photochemical reaction of the type of that undergone by quinolin-5(6*H*)-one. In turn, this justifies the observed photostability of the quinolin-5(8*H*)-one.

4. CONCLUSION

5-Hydroxyquinoline was studied by matrix isolation infrared spectroscopy, complemented by DFT(B3LYP)/6-311++G(d,p) calculations. The calculations indicated that the compound may exist in two conformers (*trans* and *cis*), differing in the orientation of the hydroxyl group. According to the calculations, the *trans* conformer (with the OH group pointing to the opposite direction of the pyridine ring of the molecule) is more stable than the *cis* form by ∼8.8 kJ mol^{-1}. Natural bond orbital and charge density analyses allowed for identification of the main factors determining the relative stability of the two conformers. On the whole, the NBO

DOI: 10.1021/acs.jpca.5b03942
J. Phys. Chem. A XXXX, XXX, XXX−XXX

interactions directly involving the OH fragment account for ~60% of the stabilization of the *trans* conformer in relation to the *cis* form, whereas the π-delocalization within the rings, which are indirectly affected by the change in the orientation of the OH group represent ~40% of the energy stabilization of the *trans* form. The NBO analysis allowed also concluding that the stabilization via the π-system is clearly dominant, accounting for ~93% of the energy stabilization, versus only ~7% due to σ NBO interactions.

The compound was isolated in an N_2-cryomatrix, at 10 K, and the analysis of the infrared spectrum of the as-deposited matrix probed the sole presence in the deposited sample of the *trans* conformer. Full assignment of the spectrum was undertaken, on the basis of the comparison between the experimental data and the calculated spectrum for *trans* 5HQ.

Broadband *in situ* UV irradiations ($\lambda \geq 288$ nm and $\lambda \geq 235$ nm) led to the observation of several chemical transformations, which were rationalized in detail through analysis of energetic data and results of TD-DFT calculations. After excitation of 5HQ to the S_1 state, homolytic cleavage of the O−H bond takes place. Subsequent reattachment of the H atom to the 5HQ radical, in the original matrix cage, led to formation of quinolin-5(6*H*)-one and quinolin-5(8*H*)-one. Although quinolin-5(6*H*)-one was found to undergo subsequent ring opening producing open-ring isomeric ketenes, quinolin-5(8*H*)-one proved to be rather stable under the used experimental conditions. The ring opening photoreaction of quinolin-5(6*H*)-one was found to be especially efficient when the irradiation was performed at higher energy ($\lambda \geq 235$ nm), due to the opening of an additional reaction channel involving the S_5 state of the molecule. As a whole, the observed photochemistry of matrix-isolated 5HQ closely matches those previously reported[22,46] for phenol and thiophenol, thus suggesting that this is a rather general pattern of photoreactivity of these types of compounds under matrix isolation conditions.

■ ASSOCIATED CONTENT

Supporting Information

Figure S1, with schemes of the postulated[20] photochemical reactions for 5HQ, 6HQ, and 7HQ isolated in Ar matrixes upon irradiation at ~300 nm. Figure S2, with schemes of the previously observed[22,46] photochemical reactions for phenol and thiophenol isolated in Ar matrixes upon UV irradiations at different wavelengths. Figures S3−S7, with the B3LYP/6-311++G(d,p) calculated infrared spectra of 5HQ radical, open-ring isomeric ketene species derived from 5HQ, Dewar 5HQ isomer, quinolin-5(7*H*)-one, and closed-ring ketene-5. Table S1, with B3LYP/6-311++G(d,p) calculated natural atomic charges for *cis* and *trans* 5HQ. Tables S2 and S3, with description of selected NBOs for *cis* and *trans* 5HQ. Table S4, with the B3LYP/6-311++G(d,p) calculated infrared spectra of 5HQ radical, open-ring isomeric species derived from 5HQ, Dewar 5HQ isomer, quinolin-5(7*H*)-one, and closed-ring ketene-5. The Supporting Information is available free of charge on the ACS Publications website at DOI: 10.1021/acs.jpca.5b03942.

■ AUTHOR INFORMATION

Corresponding Author

*N. Kus. E-mail: nkus@anadolu.edu.tr. Phone: +90 (222) 335 0580/4760.

Notes

The authors declare no competing financial interest.

■ ACKNOWLEDGMENTS

The authors thank the Portuguese Science Foundation (FCT), Lisbon, Portugal, for funding the Coimbra Chemistry Centre (FCT project PEst-OE/QUI/UI0313/2014, which is supported in part also by FEDER − European Regional Development Fund, through the COMPETE Programme, Operational Programme for Competitiveness). N. K. Acknowledges FCT for the award of a postdoctoral grant (ref SFRH/BPD/88372/2012).

■ REFERENCES

(1) Foley, M.; Tilley, L. Quinoline Antimalarials: Mechanisms of Action and Resistance and Prospects for New Agents. *Pharmacol. Ther.* **1998**, *79*, 55−87.
(2) Acton, Q. A., Ed. *Antimalarial Quinolines: Advances in Research and Application*, 2012 ed.; Scholarly Eds: Atlanta, GA, USA, 2013.
(3) Vlok, M. C. Artemisinin-Quinoline Hybrids: Design, Synthesis and Antimalarial Activity. *Ph.D. Thesis*, North-West University, Potchefstroom, 2013.
(4) Vargas, L. Y.; Castelli, M. V.; Kouznetsov, V. V.; Urbina, J. M.; Lopez, S. N.; Sortino, M.; Enriz, R. D.; Ribas, J. C.; Zacchino, S. In vitro Antifungal Activity of New Series of Homoallylamines and Related Compounds with Inhibitory Properties of the Synthesis of Fungal Cell Wall Polymers. *Bioorg. Med. Chem.* **2003**, *11*, 1531−1550.
(5) Ablordeppey, S. Y.; Fan, P.; Li, S.; Clark, A. M.; Hufford, C. D. Substituted Indoloquinolines as New Antifungal Agents. *Bioorg. Med. Chem.* **2002**, *10*, 1337−1346.
(6) Madapa, S.; Tusi, Z.; Batra, S. Advances in the Synthesis of Quinoline and Quinoline-Annulated Ring Systems. *Curr. Org. Chem.* **2008**, *12*, 1116−1183.
(7) World Health Organization. *Guidelines for the Treatment of Malaria*, Second ed.; World Health Organization: Geneva, 2010.
(8) Dorndorp, A.; Nosten, F.; Stepniewska, K.; Day, N.; White, N. and South East Asian Quinine Artesunate Malaria Trial (SEAQUAMAT) Group, Artesunate *versus* Quinine for Treatment of Severe Falciparum Malaria: a Randomised Trial. *Lancet* **2005**, *366*, 717−25.
(9) Całus, S.; Gondek, E.; Danel, A.; Jarosz, B.; Pokładko, M.; Kityk, A. V. Electro-luminescence of 6-R-1,3-diphenyl-1*H*-Pyrazolo[3,4-b]quinoline-based Organic Light-Emitting Diodes (R= F, Br, Cl, CH_3, C_2H_3 and $N(C_6H_5)_2$). *Mater. Lett.* **2007**, *61*, 3292−3295.
(10) Caeiro, G.; Lopes, J. M.; Magnoux, P.; Ayrault, P.; Ramôa Ribeiro, F. A FT-IR Study of Deactivation Phenomena in Catalytic Cracking: Nitrogen Poisoning, Coke Formation and Acidity-activity Correlations. *J. Catal.* **2007**, *249*, 234−243.
(11) Dekkers, J.; Goodwin, H. A. Multidentate Chelating Agents from Quinoline-8-aldehyde. I. Tridentate and Quadridentate Schiff Bases from Primary Diamines. *Aust. J. Chem.* **1966**, *19*, 2241−2250.
(12) Prachayasittikul, V.; Prachayasittikul, S.; Ruchirawat, S.; Prachayasittikul, V. 8-Hydroxyquinolines: a Review of Their Metal Chelating Properties and Medicinal Applications. *Drug Des., Dev. Ther.* **2013**, *7*, 1157−1178.
(13) Sirbu, D.; Consiglio, G.; Gischig, S. Palladium and Nickel Complexes of (P,N)-Ligands Based on Quinolines: Catalytic Activity for Polymerization and Oligomerization. *J. Organomet. Chem.* **2006**, *691*, 1143−1150.
(14) Fron, G. Use of Bis(8-hydroxyquinolinium) Sulfate as Fungicide on Plants. *Rev. Pathol. Entomol. Veg.* **1936**, *23*, 131−132.
(15) Liang, F.; Chen, J.; Cheng, Y.; Wang, L.; Ma, D.; Jing, X.; Wang, F. Synthesis, Characterization, Photoluminescent and Electroluminescent Properties of New Conjugated 2,2′-(Arylenedivinylene)bis-8-substituted Quinolines. *J. Mater. Chem.* **2003**, *13*, 1392−1399.
(16) Raut, S. B.; Dhoble, S. J.; Atram, R. G. Photoluminescence Studies of Trichloro-DPQ Organic Phosphor. *Adv. Mater. Lett.* **2011**, *2*, 373−376.

DOI: 10.1021/acs.jpca.5b03942
J. Phys. Chem. A XXXX, XXX, XXX−XXX

(17) Achelle, S.; Baudequin, C.; Plé, N. Luminescent Materials Incorporating Pyrazine or Quinoxaline Moieties. *Dyes Pigm.* **2013**, *98*, 575−600.
(18) Bardez, E.; Devol, I.; Larrey, B.; Valeur, B. Excited-State Processes in 8-Hydroxyquinoline: Photoinduced Tautomerization and Solvation Effects. *J. Phys. Chem. B* **1997**, *101*, 7786−7793.
(19) Karpinska, G.; Mazurek, A. P.; Dobrowolski, J. Cz. Hydroxyquinolines: Constitutional Isomers and Tautomers. *Comput. Theor. Chem.* **2011**, *972*, 48−56.
(20) Sekine, M.; Nagai, Y.; Sekiya, H.; Nakata, M. Photoinduced Hydrogen-atom Eliminations of 6-Hydroxyquinoline and 7-Hydroxyquinoline Studied by Low-Temperature Matrix-Isolation Infrared Spectroscopy and Density-Functional-Theory Calculations. *J. Phys. Chem. A* **2009**, *113*, 8286−8298.
(21) Goldman, M.; Wehry, E. L. Environmental Effects upon Fluorescence of 5- and 8-Hydroxyquinoline. *Anal. Chem.* **1970**, *42*, 1178−1185.
(22) Giuliano, B. M.; Reva, I.; Lapinski, L.; Fausto, R. Infrared Spectra and Ultraviolet-tunable Laser Induced Photochemistry of Matrix-isolated Phenol and Phenol-d_5. *J. Chem. Phys.* **2012**, *136*, 024505.
(23) Kuş, N.; Reva, I.; Bayarı, S.; Fausto, R. *In situ* Photoproduction of Dichlorodibenzo-*p*-dioxin from Non-ionic Triclosan Isolated in Solid Argon. *J. Mol. Struct.* **2012**, *1007*, 88−94.
(24) Sekine, M.; Sekiya, H.; Nakata, M. Infrared and Electronic Spectra of Radicals Produced from 2-Naphtol and Carbazole by UV-Induced Hydrogen-Atom Eliminations. *J. Phys. Chem. A* **2012**, *116*, 8980−8988.
(25) Whittle, E.; Dows, D. A.; Pimentel, G. C. Matrix Isolation Method for the Experimental Study of Unstable Species. *J. Chem. Phys.* **1954**, *22*, 1943.
(26) Fausto, R., Ed. *Low Temperature Molecular Spectroscopy*; NATO-ASI Series C483; Kluwer: Amsterdam, 1996.
(27) Fausto, R.; Gómez-Zavaglia, A. Light Induced Reactions in Cryogenic Matrices (Highlights 2011−2012). In *Photochemistry, A Specialist Periodic Report*; Albini, A., Fasani, E., Eds.; RSC Publishing: London, 2013; Vol. *41*, p 12.
(28) Frisch, M. J.; Trucks, G. W.; Schlegel, H. B.; Scuseria, G. E.; Robb, M. A.; Cheeseman, J. R.; Scalmani, G.; Barone, V.; Mennucci, B.; Petersson, G. A.; et al. *Gaussian 09*, Revision A.0.2; Gaussian, Inc.: Wallingford, CT, 2009.
(29) McLean, A. D.; Chandler, G. S. Contracted Gaussian Basis Sets for Molecular Calculations. I. Second Row Atoms. Z=11−18. *J. Chem. Phys.* **1980**, *72*, 5639−5648.
(30) Becke, A. D. Density Functional Exhange-Energy Approximation with Correct Asymptotic Behavior. *Phys. Rev. A: At., Mol., Opt. Phys.* **1988**, *38*, 3098−3100.
(31) Lee, C. T.; Parr, R. G. Development of the Colle Salvetti Correlation-Energy Formula into a Functional of the Electron Density. *Phys. Rev. B* **1988**, *37*, 785−789.
(32) Vosko, S. H.; Wilk, L.; Nusair, M. Accurate Spin-Dependent Electron Liquid Correlation Energies for Local Spin Density Calculations: A Critical Analysis. *Can. J. Phys.* **1980**, *58*, 1200−1211.
(33) Weinhold, F.; Landis, C. R. Valency and Bonding. *A Natural Bond Orbital Donor-Acceptor Perspective*; Cambridge University Press: New York, 2005.
(34) Reed, A. E.; Curtiss, L. A.; Weinhold, F. Intermolecular Interactions from a Natural Bond Orbital, Donor-acceptor Viewpoint. *Chem. Rev.* **1988**, *88*, 899−926.
(35) Bauernschmitt, R.; Ahlrichs, R. Treatment of Electronic Excitations Within the Adiabatic Approximation of Time Dependent Density Functional Theory. *Chem. Phys. Lett.* **1996**, *256*, 454−464.
(36) Stratmann, R. E.; Scuseria, G. E.; Frisch, M. J. An Efficient Implementation of Time-Dependent Density-Functional Theory for the Calculation of Excitation Energies of Large Molecules. *J. Chem. Phys.* **1998**, *109*, 8218−8224.
(37) Mukherjee, A.; Tothadi, S.; Chakraborty, S.; Ganguly, S.; Desiraju, G. R. Synthon Identification in Co-crystals and Polymorphs with IR Spectroscopy. Primary Amides as a Case Study. *CrystEngComm* **2013**, *15*, 4640−4654.
(38) Reva, I. D.; Stepanian, S. G.; Adamowicz, L.; Fausto, R. Missing Conformers: Comparative Study of Conformational Cooling in Cyanoacetic Acid and Methyl Cyanoacetate Isolated in Low Temperature Inert Gas Matrixes. *Chem. Phys. Lett.* **2003**, *374*, 631−638.
(39) Fausto, R. Bonding in Carbonyl and Thiocarbonyl Compounds: An Ab Initio Charge Density Study of H_2C=X and HC(=X)YH (X,Y= O or S). *J. Mol. Struct.: THEOCHEM* **1994**, *315*, 123−136.
(40) Fausto, R.; Batista de Carvalho, L. A. E.; Teixeira-Dias, J. J. C.; Ramos, M. N. The *s-cis* and *s-trans* Conformers of Formic, Thioformic and Dithioformic Acids: an Ab Initio Study. *J. Chem. Soc., Faraday Trans. 2* **1989**, *85*, 1945−1962.
(41) Boule, P.; Richard, C.; David-Oudjehani, K.; Grabner, G. Photochemical Behaviour of Halophenols in Aqueous Solution. *Proc. - Indian Acad. Sci., Chem. Sci.* **1997**, *109*, 509−519.
(42) Bonnichon, F.; Richard, C.; Grabner, G. Formation of an α-Ketocarbene by Photolysis of Aqueous 2-Bromophenol. *Chem. Commun.* **2001**, 73−74.
(43) Akai, N.; Kudoh, S.; Takayanagi, M.; Nakata, M. Photoreaction Mechanisms of 2-Bromophenols Studied by Low-Temperature Matrix-Isolation Infrared Spectroscopy and Density-Functional-Theory Calculations. *Chem. Phys. Lett.* **2002**, *363*, 591−597.
(44) Bell, G. A.; Dunkin, I. R. Tetrachlorocyclopentadienylidene, Indenylidene and Fluorenylidene in Low-Temperature Matrices. Ultraviolet and Infrared Spectra and Reactions with Carbon Monoxide. *J. Chem. Soc., Faraday Trans. 2* **1985**, *81*, 725−734.
(45) Tidwell, T. T. Aryl Hetaryl Ketenes. In *Ketenes and Derivatives*; Danheiser, R. L., Ed.; Vol. *23* of Science of Synthesis; Thieme: Stuttgart, 2006; Chapter 23.12, pp 391−492.
(46) Reva, I.; Nowak, M. J.; Lapinski, L.; Fausto, R. Hydrogen Atom Transfer Reactions in Thiophenol: Photogeneration of Two New Thione Isomers. *Phys. Chem. Chem. Phys.* **2015**, *17*, 4888−4898.
(47) Kuş, N.; Breda, S.; Fausto, R. In Situ Direct Photoproduction of Ketenes from Substituted Coumarins Isolated in Solid Argon: The Case of N-(2-oxo-2*H*-chromen-3-yl)acetamide. *J. Mol. Struct.* **2009**, *924−926*, 81−88.
(48) Breda, S.; Reva, R.; Lapinski, L.; Fausto, R. Matrix-Isolation FTIR and Theoretical Study of the UV-Induced Photochemistry of α-Pyrone. *Phys. Chem. Chem. Phys.* **2004**, *6*, 929−937.
(49) Wu, L.; Lambo, R.; Tan, Y.; Liu, A.-W.; Hu, A.-M. Infrared Spectroscopy of CO Isolated in Solid Nitrogen Matrix. *Chin. J. Chem. Phys.* **2014**, *27*, 54−8.
(50) Jacox, M. E.; Milligan, D. E. Matrix Isolation Study of the Vacuum Ultraviolet Photolysis of Allene and Methylacetylene Vibrational and Electronic Spectra of the Species C_3, C_3H, C_3H_2, and C_3H_3. *Chem. Phys.* **1974**, *4*, 45−61.
(51) Santos, R. M. B.; Simões, J. A. M. Energetics of the O—H Bond in Phenol and Substituted Phenols. A Critical Evaluation of Literature Data. *J. Phys. Chem. Ref. Data* **1998**, *27*, 707−739.
(52) Wright, J. S.; Carpenter, D. J.; McKay, D. J.; Ingold, K. U. Theoretical Calculation of Substituent Effects on the O−H Bond Strength of Phenolic Antioxidants Related to Vitamin E. *J. Am. Chem. Soc.* **1997**, *119*, 4245−4252.
(53) Lide, D. R., Ed. *CRC Handbook of Chemistry and Physics*, 78th ed.; CRC Press: New York, 1997−1998.
(54) Chandra, A. K.; Uchimaru, T. The O−H Bond Dissociation Energies of Substituted Phenols and Proton Affinities of Substituted Phenoxide Ions: A DFT Study. *Int. J. Mol. Sci.* **2002**, *3*, 407−411.

DOI: 10.1021/acs.jpca.5b03942
J. Phys. Chem. A XXXX, XXX, XXX−XXX